Abstract

Title of Dissertation: Of Plerions and Supernova Remnants:
γ-Ray Observations of the Stellar Graveyard.

Jamie Michael Cohen, Doctor of Philosophy, 2016

Dissertation directed by: Doctor Elizabeth Hays
Astroparticle Physics Laboratory, Code 661
NASA Goddard Space Flight Center

Professor M. Coleman Miller
Department of Astronomy
University of Maryland

Here I shall abstract!

Of Plerions and Supernova Remnants:
γ-Ray Observations of the Stellar Graveyard.

by

Jamie Michael Cohen

Dissertation submitted to the Faculty of the Graduate School of the
University of Maryland at College Park in partial fulfillment
of the requirements for the degree of
Doctor of Philosophy
2016

Advisory Committee:

Doctor Elizabeth Hays, Advisor
Professor M. Coleman Miller, Chair/Advisor
Professor Christopher S. Reynolds
Professor Derek C. Richardson
Doctor Who

Preface

Brief description of the content of this thesis. Statements about which chapters (or parts of) have been published where. Reference like Part of Chapter 1

To Vanessa!

Acknowledgements

I should probably thank someone.

Contents

List of Tables

List of Figures

Chapter 1

Introduction

"Maybe I'll have a super relevant quote here!"

—by some awesome human, from *Some book*

1.1 Goooo γ-rays go!

Overview of the entire thesis, why gamma-rays, why the LAT, why SNRs and PWN and extended sources.

1.2 Dissertation Overview

Chapter 2

Gamma-ray Astronomy

history

gamma-rays, gamma-ray astronomy, gamma-ray sky

gamma-ray production mechanisms

gamma-ray telescopes leads into the LAT, Egret was predecessor , what it did and what were some relevant unanswered questions regarding supernova remnants

Maybe combine the telescope stuff with the LAT section and leave this section for history and astrophysics of γ-rays? Or just combine this section with LAT section?

Chapter 3

The Fermi Gamma Ray Space Telescope

Maybe combine this with the γ-ray astro section?

3.1 Overview

General info about Fermi, when it was conceived, launched, what questions it was designed to address etc.

3.2 The Large Area Telescope

Details on the LAT and it's design, be sure to focus on things that particularly pertain to the work I've done like what determines the PSF, thing about Pass 8 here maybe? Or maybe later on.

what science was it designed to answer

general capabilities

details about aspect of the LAT related to extended sources, what determines

PSF

Searching for extended Galactic sources leads into stellar remnants section?

Chapter 4

Stellar Remnants

Is it weird to call them stellar remnants? It's not like the remnant of the star, but of the supernova

4.1   Supernova Remnants

History of SNR, radio detections, then x-ray, can't really ID in new ones with the LAT, theory: snow plow , ST evolution, radiative phase, shell type, mixed morphology (shell plus center filled thermal x-ray)

4.2   Pulsar Wind Nebulae

How much of my thesis is really about pwn? in 2FHL we detect some. if including above 10gev work, they'll be there too. Much of the thesis is really about extended gamma-ray sources, but not sure how that fits into the title and chapters yet

Do I need to get into composite SNRs (I think composite means SNR + PWN right?) Maybe relevant for G150? Some things about interaction of reverse shock with PWN and crushing/reverberations of the PWN?

How we detect gamma-rays from SNRs/PWNe in the Galaxy leads to and analysis section maybe?

Chapter 5

Analysis of *Fermi*-LAT - data

I'm not sure about this chapter yet. Maybe it's a general section on Analysis of Fermi data, why maximum likelihood, how it's formulated, implemented in the Science Tools, pointlike and the analysis for extended sources

5.1   addSrcs

Chapter 6

The 1st *Fermi*-LAT Supernova Remnant Catalog

Application of addSrcs searching for point sources, fitting single extended source, results on detected SNRs and population properties, implications for total power in cosmic rays

How much of the SNR cat paper can I put in as is, how much can I take with modifications? Below is just the addSrcs section and appendix A

6.1 Input Source Model Construction

To characterize each candidate SNR we constructed a model of γ-ray emission in the RoI which includes all significant sources of emission as well as the residual background from CRs misclassified as γ-rays. We implemented an analysis method to create and optimize the [JAM: fill this in] models for each of the 279 RoIs. For each RoI, we started with all sources listed in the Second *Fermi* LAT catalog (2FGL) (**?**), based on 2 years of Source class data, within the RoI. To this we add pulsars from the LAT Second Pulsar Catalog (2PC) (**?**), based on 3 years of source class data, with

2PC taking precedence for sources that exist in both. For the diffuse emission we combined the standard IEM corresponding to our P7 data set, gal_2yearp7v6_v0.fits, with the standard model for isotropic emission, which accounts for extragalactic diffuse γ-ray emission and residual charged particles misclassified as γ-rays. Both the corresponding isotropic model, iso_p7v6source.txt, and the IEM are the same as used for the 2FGL catalog analysis[1].

Compared to 2FGL, we used an additional year of data and limited the energy range to $1 - 100\,\mathrm{GeV}$. This can result in different detection significances and localizations than previously reported in 2FGL. To account for these effects, we recreated the RoIs' inner $3°$ radius regions, which encompass the radio extents of all known SNRs, observed to be $\leq 2.6°$ and allows a margin for the LAT PSF. The weighted average 68% containment radius of the LAT PSF for events at $1\,\mathrm{GeV}$ is $\sim 0.7°$ (**?**). We note that this implicitly assumes that an SNR's GeV extent should not be more than about an order of magnitude larger than its radio extension and also note that the selection biases stated in Green's catalog limit the range of known SNRs' radio extensions.

To build the inner $3°$ radius model of each RoI, we first removed all sources except identified Active Galactic Nuclei (AGN) and pulsars, whose positions on the sky are independently confirmed by precise timing measurements (**?**). Retained AGN were assigned their 2FGL positions and spectral model forms. Pulsars' positions and spectral forms were taken from 2PC. 2FGL sources identified or associated with SNRs are removed when they lie within the inner $3°$.

We generated a map of source test statistic (TS) defined in **?** via `pointlike` on a square grid with $0.1° \times 0.1°$ spacing that covers the entire RoI. `pointlike`

---

[1]Further details on the diffuse emission models are available at `http://fermi.gsfc.nasa.gov/ssc/data/access/lat/BackgroundModels.html`

employs a binned maximum likelihood method. The source TS is defined as twice the logarithm of the ratio between the likelihood $\mathcal{L}_1$, here obtained by fitting the model to the data including a test source, and the likelihood $\mathcal{L}_0$, obtained here by fitting without the source, i.e., $\mathrm{TS} = 2\log(\mathcal{L}_1/\mathcal{L}_0)$. At the position of the maximum TS value, we added a new point source with a Power Law (PL) spectral model:

$$\frac{dN}{dE} = N\frac{(-\Gamma + 1)E^{-\Gamma}}{E_{\max}^{-\Gamma+1} - E_{\min}^{-\Gamma+1}} \qquad (6.1)$$

where N is the integrated photon flux, Γ is the photon index, and $E_{\min}$ and $E_{\max}$ are the lower and upper limit of the energy range in the fit, set to $1\,\mathrm{GeV}$ and $100\,\mathrm{GeV}$, respectively. We then performed a maximum likelihood fit of the RoI to determine N and Γ and localized the newly added source. The significance of a point source with a PL spectral model is determined by the χ_n^2 distribution for n additional degrees of freedom for the additional point source, which is typically slightly less than $\sqrt{\mathrm{TS}}$[2].

To promote consistent convergence of the likelihood fit, we limited the number of free parameters in the model. For sources remaining after the removal step, described above, we freed the normalization parameters for the sources within $5°$ of the RoI center, including identified AGN and pulsars. For 2FGL sources between $5°$ and $10°$, we fixed all parameters. The spectrum of the IEM was scaled with a PL whose normalization and index were free, as done in 2FGL. For the isotropic emission model, we left the normalization fixed to the global fit value since the RoIs are too small to allow fitting the isotropic and Galactic IEM components independently. The isotropic component's contribution to the total flux is small compared to the IEM's at low Galactic latitudes.

After localizing them, the new sources were tested for spectral curvature. In each

---

[2]See http://fermi.gsfc.nasa.gov/ssc/data/analysis/documentation/Cicerone/Cicerone_Likelihood/T for further details.

of the 4 energy bands per decade we calculated the TS value for a PL with spectral index fixed to 2 and then summed the TS values. We refer to this as $\text{TS}_{\text{bandfits}}$. A value for $\text{TS}_{\text{bandfits}}$ much greater than the TS calculated with a PL (TS_{PL}) suggests with a more rapid calculation that the PL model may not accurately describe the source. Analogously to 2FGL (**?**), we allow for deviations of source spectra from a PL form by modeling sources with a log-normal model known colloquially as LogParabola or logP:

$$\frac{dN}{dE} = N_0 \left(\frac{E}{E_b} \right)^{-(\alpha + \beta \log(E/E_b))} \tag{6.2}$$

where N_0 is the normalization in units of photons/MeV, α and β define the curved spectrum, and E_b is fixed to $2\,\text{GeV}$. If $\text{TS}_{\text{bandfits}} - \text{TS}_{\text{PL}} \geq 25$, we replaced the PL spectral model with a logP model and refit the RoI, including a new localization step for the source. We retained the logP model for the source if the global $\log \mathcal{L}$ across the full band improved sufficiently: $\text{TS}_{\text{curve}} \equiv 2(\log \mathcal{L}_{\text{logP}} - \log \mathcal{L}_{\text{PL}}) \geq 16$. Otherwise we returned the source to the PL model which provided the better global $\log \mathcal{L}$. Across all RoIs, less than 2% of the newly added sources retained the logP model.

We continued iteratively generating TS maps and adding sources within the entire RoI until additional new sources did not significantly change the global likelihood of the fit. The threshold criterion was defined as obtaining $\text{TS} < 16$ for three consecutively added new sources, denoted as $\text{N}_{\text{TS}<16} = 3$. Despite iteratively adding a source at the location of the peak position in the TS map, the TS values of new sources may not decrease monotonically with iteration for several reasons. First, source positions were localized after fitting the RoI and generating the TS map. Second, some added sources were fit with a more complex spectral model than a simple PL. Finally, when creating the TS map, we fixed the source's spectral index to 2, whereas when adding the actual source to the model, we allowed its index to vary.

The specific value of $N_{TS<16} = 3$ was chosen to avoid missing sources with $TS \geq 25$, the threshold commonly used for source detection in LAT data, and to optimize computation time. We tested the threshold by selecting eight representative SNRs from both complex and relatively simple regions of the sky, with both hard and soft spectral indices. We applied the above procedure to the test RoIs using a criterion of $N_{TS<16} = 6$ and counted how many $TS \geq 25$ sources would be excluded if a smaller $N_{TS<16}$ criterion was used. Reducing the threshold to $N_{TS<16} = 3$ cut only one significant source in any of the regions. Since the maximum number of sources added in any test RoI was 38, the minimum 14, and the total number of sources added across all test regions was 221, we chose to use $N_{TS<16} = 3$ for the full sample. To allow for proper convergence of the likelihood fit, we reduced the number of free parameters prior to each new source addition. If the previously added source was between $3°$ and $5°$ of the center of the RoI, just its normalization was freed, and if greater than $5°$ all its source parameters were fixed.

To avoid having newly added sources overlap with pulsars, we deleted new sources from the RoI if they were within $0.2°$ of a γ-ray pulsar and refit the pulsar in the $1 - 100\,\text{GeV}$ range following the 2PC conventions. 2PC modeled pulsar spectra as PL with an exponential cutoff (PLEC),

$$\frac{dN}{dE} = N_0 \left(\frac{E}{E_0}\right)^{-\Gamma} \exp\left(-\frac{E}{E_c}\right)^b, \tag{6.3}$$

where N_0 is the normalization factor, Γ is the photon spectral index, E_c the cutoff energy, and b determines to the sharpness of the cutoff. 2PC assessed the validity of fixing b to 1 in Equation 6.3 (PLEC1) by repeating the analysis using a PL model, as well as the more general exponentially cut off PL form, allowing the parameter b in Equation 6.3 to vary. For the pulsar spectra in this analysis, we compared the maximum likelihood values for spectral models with and without a cutoff and with and without the value of b being free, via $TS_{cut} \equiv 2(\log \mathcal{L}_{PLEC1} - \log \mathcal{L}_{PL})$ and

$\text{TS}_b \equiv 2(\log \mathcal{L}_{\text{PLEC}} - \log \mathcal{L}_{\text{PLEC1}})$ to determine which to use. If $\text{TS}_{\text{cut}} < 9$ is reported for the pulsar in 2PC then a PL model is used. If $\text{TS}_{cut} \geq 9$, we then check to see if the cutoff energy fit in 2PC lies within the restricted energy range of $1 - 100\,\text{GeV}$ used in this work. For pulsars with cutoffs $\geq 1\,\text{GeV}$, we then use the PLEC model if $\text{TS}_b \geq 9$, and the PLEC model with cutoff freed otherwise. For those pulsars with cutoffs less than 1 GeV the spectral parameters are fixed to the 2PC values.

To complete the construction of our point source RoI model, we took the output of the previous steps and removed all sources with $\text{TS} < 16$. This final model was then used as the starting model for analyzing candidate SNR emission. We conservatively allow sources with TS down to 16 ($\sim 4\,\sigma$) in order to account for the effects of at least the brightest sub-threshold sources on the parameter fits for the other sources in the model. Furthermore, while the SNR analysis method described in the next subsection (**??**) is allowed to remove sources, it cannot add them. Thus we start from a set of sources designed to allow the final model to capture all significant emission within the central region. To corroborate our method of systematically adding sources to a region, we compare our RoI source models with those found by the 2FGL approach in Appendix 6.2.

6.2   Comparison of Source Models with 2FGL

This SNR catalog was constructed using 3 years of P7 Source class data in the energy range $1 - 100\,\text{GeV}$, whereas 2FGL used $2\,\text{years}$ of data over the larger energy range $0.1 - 100\,\text{GeV}$. The differences in observing time and energy range resulted in residual, unmodeled emission in some RoIs as well as changes to some 2FGL sources' spectral model, position localization, and detection significance. Here we compare the input source models constructed for this catalog, described in Section 6.1, with

2FGL to better understand the method's ability to describe the regions studied. Since we rederive the input source model only within a 3° radius of the center of each RoI, we consider sources only inside that radius.

Given the data set differences, in each RoI we expect similar but not identical numbers of sources relative to those in 2FGL. Figures 6.1 and 6.2 show the numbers of significant (TS ≥ 25) 2FGL sources and derived input model sources (excluding 2FGL identified AGN and pulsars kept in the input model) in individual RoIs as 2D histograms. In Figure 6.1, the number of sources in the derived input model is typically greater than the number of 2FGL sources that are significant at $1 - 100\,\mathrm{GeV}$. 73 of the 279 RoIs studied contain at least one of the the 12 extended 2FGL sources. Since 2FGL extended sources were removed from the inner 3° of each RoI, and this region was repopulated with point sources, we can detect multiple point sources inside the extent of any removed extended 2FGL sources. This decomposition of extended sources, combined with the longer data set and different energy range compared to 2FGL, contribute to the high ratio of input model to 2FGL sources in some RoI, which demonstrates the need to rederive the source model.

To more accurately represent the 2FGL sources being reproduced in the central 3°, in Figure 6.2 we limited the input model sources to those within 0.2° (approximately the width of the core of the $10\,\mathrm{GeV}$ PSF) of a 2FGL source, effectively excluding input sources that are not co-spatial with a 2FGL source. Here we see that the majority of 2FGL sources have counterparts in the rederived set. As a region's complexity increases, seen as an increase in numbers of 2FGL sources, up to about half of the 2FGL sources may not have counterparts within 0.2°. Given that in these same regions we have more new sources than 2FGL sources, as seen in Figure 6.1, we find as expected that the longer data set with improved statistics at higher energies, where the angular resolution of the LAT is the best, allows us to
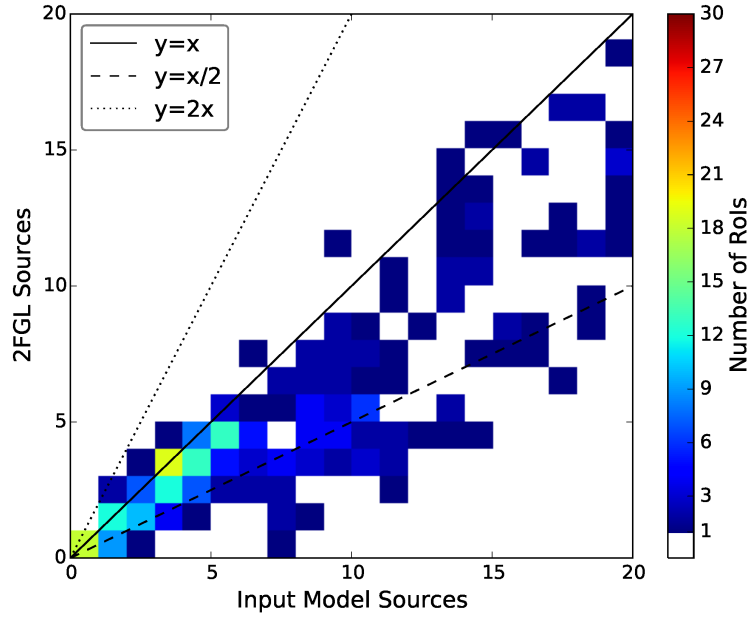
14

Figure 6.1: Comparison of the number of 2FGL sources with $\mathrm{TS}_{1-100\,\mathrm{GeV}} \geq 25$ (excluding AGN and pulsars) with the number of newly added input model sources in the present analysis, for sources within $3°$ of the center of each RoI. The color scale shows the number of RoIs with a particular combination of numbers of 2FGL sources and new sources. White corresponds to no RoI with that combination of source counts.

add new sources to account for newly significant excesses in these complex regions. Additionally, sources with low TS in 2FGL are particularly susceptible to having a newly added source which may start at a similar position but then localize further than $0.2°$ from the 2FGL source.

Thus, we find that the method developed and used here produces a model which reproduces the 2FGL sources as expected, including differences that trend as anticipated given the longer data set and modified energy range, yielding better spatial resolution. The new method thus provides reasonable representations of the regions being modeled as input for the final analysis.
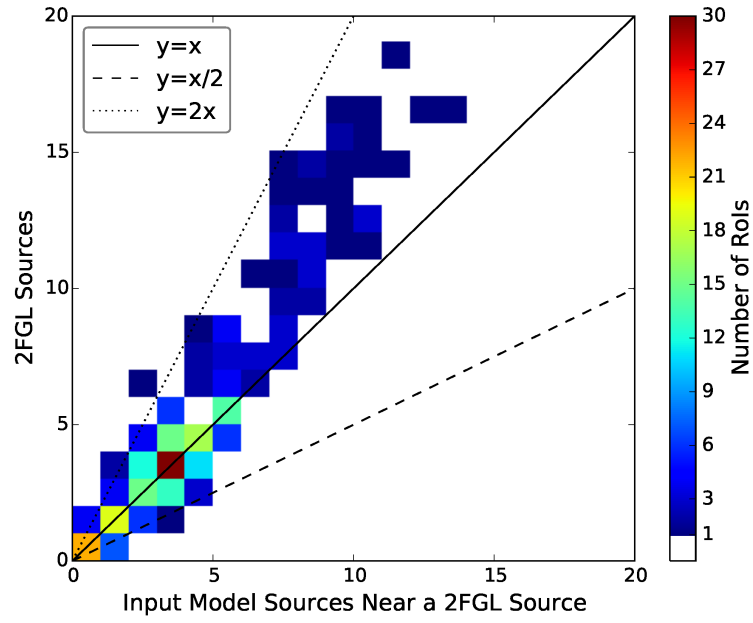
Figure 6.2: Same as Figure 6.1, including only input model sources lying within 0.2° of a 2FGL source.

Chapter 7

2FHL: The Second Catalog of

Hard *Fermi*-LAT Sources

Application of addSrcs searching for extended (and really point too) sources in the sky. 2FHL results on all Galactic sources. Index histograms for entire 2FHL population showing harder index for Galactic soures

How much of the 2FHL paper can I put in as is, how much can I take with modifications?

Below is if I just took the sections describing extend sources.

7.1   Extended Sources Previously Detected by the LAT

We explicitly modeled sources as spatially extended when a previous, dedicated, analysis found the source to be resolved by the LAT. The 25 extended sources reported in 3FGL were included in our model using the spatial templates derived in the individual source studies (see references in Acero et al. 2015). Refitting

the positions and extensions of the 3FGL extended sources in this energy range is beyond the scope of this work.

Of the 25 3FGL extended sources, 19 are significantly detected here above the detection threshold (TS $\geq$ 25). Only 6 sources are not detected and, since all have TS < 10, are removed from the sky model (see §7.3 for details).

One extended LAT source has had a dedicated analysis published since the release of the 3FGL catalog. Abramowski et al. (2015a) reported joint H.E.S.S. and LAT observations of the very high energy (VHE) source HESS J1834-087. This source is coincident with supernova remnant (SNR) W41 and was detected as spatially extended in a wide energy range spanning 1.8 GeV to 30 TeV. In this paper, we employ the spatial model for the GeV emission determined in Abramowski et al. (2015a), leading to a significant detection of this source.

7.2 Newly Detected Extended Sources

In addition to modeling the extended sources mentioned in §7.1, we performed a blind search of the Galactic plane ($|b| < 10°$) to identify potential extended sources not included in previously published works. Our analysis pipeline is similar to that used in Hewitt et al. (2013), with some modifications tailored to searching for multiple extended sources in an ROI. The pipeline employs the `pointlike` binned maximum likelihood package (Kerr 2010), in particular utilizing the extended source fitting tools validated by Lande et al. (2012) to simultaneously fit the position, extension, and spectra of sources in our ROI.

We created 72 ROIs of radius 10°, centered on b $= 0°$ with neighboring ROIs overlapping and separated by 5° in Galactic longitude. Our initial model of the γ-ray emission in each ROI consisted solely of the Galactic diffuse (allowing just the

normalization to be fit) and isotropic emission models (fixing the normalization), with no other sources in the ROI. Emission in the ROIs was further characterized by adding sources and fitting their spectral parameters (normalization and spectral index) in a $14° \times 14°$ region.

A TS map, that included all significant sources found previously, made up of $0.1° \times 0.1°$ bins across the ROI, was created at each iteration and a small radius $(0.1°)$ uniform disk, with a power-law spectrum was placed at the position of the peak TS pixel. The spectra of any newly added sources, as well as the position, extension, and spectral parameters of the disk were then fit. If $\text{TS}_{\text{ext}} \geq 16$, where $\text{TS}_{\text{ext}} = 2 \log(\mathcal{L}_{\text{ext}}/\mathcal{L}_{\text{ps}})$ (i.e. twice the logarithm likelihood ratio of an extended to a point source, Lande et al. 2012), then the disk was kept in the model. For $\text{TS}_{\text{ext}} < 16$, the extended source was replaced by a point source with a power-law spectral model. For the point-source replacement case, spectral parameters of sources in the ROI were fit and the position of the new point source was optimized. Finally, the spatial parameters of any previously added extended sources were refit iteratively before creating a new TS map and repeating the process. We stopped adding sources when the peak TS was less than 16 for two successive sources.

To assess the impact of fitting extended sources when starting with an ROI devoid of sources, a crosscheck analysis (also using `pointlike`) was performed across the Galactic plane. We included 3FGL point and extended sources, the Galactic diffuse and isotropic emission, and pulsars from the second *Fermi*-LAT pulsar catalog (Abdo et al. 2013) (as well as from 3FGL) in the preliminary source model for each region. Sources were iteratively added to account for residual emission and both these residual sources and 3FGL sources were tested for extension. Remarkably, this alternative analysis converges (i.e. spectral and spatial parameters for the detected extended sources are compatible in both analyses) to the initially

source-devoid analysis for nearly all detected extended sources.

Extended sources detected in the analysis described in this section for which the position and extension were compatible with those found by the crosscheck were included in the ROI model at step 1 of the full ML analysis detailed in §**??**. Seed point sources interior to the extended sources were removed prior to the ML fit. To address the ambiguity between detecting a source as spatially extended as opposed to a combination of point sources, we utilized the algorithm detailed in Lande et al. (2012) to simultaneously fit the spectra and positions of two nearby point sources. We only consider a source to be extended if $TS_{ext} > TS_{2pts}$ (improvement when adding a second point source). Our blind search of the Galactic plane allowed us to find 5 sources not previously detected as extended by *Fermi*-LAT. Further details on these sources are presented in § 7.3.

7.3 Extended Source Results

In total, 31 sources are modeled as spatially extended and input into the ML analysis: 25 listed in 3FGL, 5 sources detected in the `pointlike` analysis (described in § 7.1) that were not detected as extended at the time of 3FGL, and one, SNR W41, reported recently by both the H.E.S.S. and LAT teams (Abramowski et al. 2015a). Names and properties of the extended sources are provided in Tables 7.1 and 7.2. Six extended sources, detected in 3FGL, were not detected in 2FHL: the SMC, S 147 (the point source 2FHL J0534.1+2753 was detected inside it), the lobes of Centaurus A (although we detect its core as a point source, 2FHL J1325.6−4301), W 44, HB 21 and the Cygnus Loop.

We detect a weak source, 2FHL J1714.1−4012 (TS = 27), just outside the southwestern edge of the 3FGL spatial template used to model the emission from SNR

RX J1713.7−3946 (2FHL J1713.5−3945e). 2FHL J1714.1−4012 has a hard spectral index $\Gamma = 1.63 \pm 0.38$, that is within errors of the spectral index derived for the SNR, $\Gamma = 2.03 \pm 0.20$. It is unclear whether 2FHL J1714.1−4012 is a distinct source separated from the SNR, or the result of un-modeled residual emission due to an imperfection in the spatial template adopted for the extended source.

2FHL J1836.5−0655e is associated with the PWN HESS J1837−069. The 3FGL catalog contains several point sources in the vicinity of the PWN. We detect three sources in the vicinity, 2FHL J1834.5−0701, 2FHL J1837.4−0717 and 2FHL J1839.5−0705, the first two of which are coincident with 3FGL sources (3FGL J1834.6−0659, 3FGL J1837.6−0717 respectively). The power-law spectral indices of the three 2FHL point sources and 2FHL J1836.5−0655e are all consistent with each other. The concentration of sources around HESS J1837−069 combined with the spectral compatibility of the sources is suggestive of a common origin to the γ-ray emission in this region. However, the surrounding γ rays could arise from other sources in the region (Gotthelf & Halpern 2008); further analysis is necessary to determine the nature of the sources in this region.

A brief description of the five new 2FHL extended sources is given below with residual TS maps for the region surrounding each source shown in Figure 7.1. Detailed analyses of these new extended sources will be reported in separate papers.

2FHL J1443.2−6221e overlaps with the young, radio-detected SNR RCW 86 (G315.42.3). RCW 86 is a $42'$ diameter SNR that lies at a distance of 2.3-2.8 kpc and is likely associated with the first recorded supernova, SN 185 AD (Rosado et al. 1996; Sollerman et al. 2003). With more than 40 months of data and using the `P7SOURCE` dataset, the LAT did not significantly detect the SNR, but upper limits on detection at GeV energies combined with detection of significant extension in the TeV (Aharonian et al. 2009) were sufficient to strongly favor a leptonic origin

21

for the emission (Lemoine-Goumard et al. 2012).

An updated LAT analysis of RCW 86 using 76 months of data, as well as the Pass 8 event-level analysis, resulted in detection of the SNR by the LAT as well as significant extension measurement (Hewitt & Fermi-LAT Collaboration 2015). In this paper, we report the results derived for 2FHL J1443.2−6221e from the `pointlike` analysis described in § 7.1.

2FHL J1419.2−6048e is a newly detected extended sources with size $\sigma_{\mathrm{disk}} = 0.36°\pm$ 0.03°, that overlaps two nearby PWN/PSR complexes in the Kookaburra region. In the southwest of Kookaburra, HESS J1418−609 (Aharonian et al. 2006) is coincident with both the extended non-thermal X-ray "Rabbit" PWN (G313.3+0.1, Roberts et al. 1999), and the γ-ray detected pulsar PSR J1418−6058 (Abdo et al. 2009). The northeast region, called "K3", contains HESS J1420−607, coincident with PWN G313.5+0.3 and PSR J1420−6048. Acero et al. (2013) detected, with *Fermi*-LAT , emission from both HESS J1418−609 (with a soft spectral index, pulsar-like spectrum) and HESS J1420−607 (with a hard power-law index) above 10 GeV, but only HESS J1420−607 was significantly detected above 30 GeV. Neither showed significant extension. Our result for the fitted power-law spectral index of 2FHL J1419.2−6048e is in agreement with the previous GeV and TeV results, yet our measured radius is considerably larger than the TeV extension. To compare the extensions of the uniform disk model used for 2FHL J1419.2−6048e in this paper to the Gaussian model of Aharonian et al. (2006), we defined the radius which contains 68% of the source's intensity as r_{68}, with $r_{68,\mathrm{Gaussian}} = 1.51\sigma$, and $r_{68,\mathrm{disk}} = 0.82\sigma$ (Lande et al. 2012). We find that $r_{68} \simeq 0.30°$ for 2FHL J1419.2−6048e, and $r_{68} \simeq$ 0.09° for HESS J1420−607.

2FHL J1355.2−6430e, coincident with the VHE source HESS J1356−645, is detected as extended ($\sigma_{\mathrm{disk}} = 0.57° \pm 0.02°$) for the first time by the LAT in this

work. The source HESS J1356−645 (Abramowski et al. 2011) is associated with the pulsar PSR J1357−6429, which was determined to be powering a surrounding extended radio and X-ray PWN (Lemoine-Goumard et al. 2011). Acero et al. (2013) detected faint emission from the nebula, and derived a 99% c.l. Bayesian upper limit on extension ($\sigma_{\mathrm{Gauss}} < 0.39°$) in the absence of significant extension. The fitted spectral index for 2FHL J1355.2−6430e is compatible with the GeV and TeV results (Abramowski et al. 2011; Acero et al. 2013), however, the fitted disk extension is larger than that of the TeV detection, with $r_{68} \simeq 0.47°$ for 2FHL J1355.2−6430e and $r_{68} \simeq 0.30°$ for HESS J1356−645.

2FHL J1112.4−6059e is an extended source ($\sigma_{\mathrm{disk}} = 0.53° \pm 0.03°$) newly detected by the LAT that encircles two 3FGL sources, 3FGL J1111.9−6058 and 3FGL J1111.9−6038, and has another, 3FGL J1112.0−6135, just outside its boundary (Acero et al. 2015). The extended source also partially overlaps the massive star forming region NGC 3603.

Finally, **2FHL J0431.2+5553e** is a large extended source ($\sigma_{\mathrm{disk}} = 1.27° \pm 0.04°$), with a hard spectrum, that has not been previously detected at γ-ray energies. It overlaps the recently discovered radio SNR G150.3+4.5 (Gao & Han 2014). G150.3+4.5 is a $2.5° \times 3°$ (Galactic coordinates) elliptical shell type SNR that has a steep radio synchrotron spectrum ($\alpha = -0.6$), indicative of radio SNRs.

Table 7.1.   2FHL extended sources previously detected by the *Fermi*-LAT

2FHL Name	l [deg]	b [deg]	TS	Association	Class	Spatial model	Extension [deg]
J0526.6−6825e	278.843	-32.850	49.80	LMC	gal	2D Gaussian	1.87
J0617.2+2234e	189.048	3.033	398.64	IC 443	snr	2D Gaussian	0.27
J0822.6−4250e	260.317	-3.277	63.87	Puppis A	snr	Disk	0.37
J0833.1−4511e	263.333	-3.104	49.70	Vela X	pwn	Disk	0.91
J0852.8−4631e	266.491	-1.233	437.21	Vela Jr	snr	Disk	1.12
J1303.4−6312e	304.235	-0.358	56.06	HESS J1303−631	pwn	2D Gaussian	0.24
J1514.0−5915e	320.269	-1.276	165.51	MSH 15−52	pwn	Disk	0.25
J1615.3−5146e	331.659	-0.659	128.15	HESS J1614−518	spp	Disk	0.42
J1616.2−5054e	332.365	-0.131	87.18	HESS J1616−508	pwn	Disk	0.32
J1633.5−4746e	336.517	0.121	114.17	HESS J1632−478	pwn	Disk	0.35
J1713.5−3945e	347.336	-0.473	60.98	RX J1713.7−3946	snr	Map	0.56
J1801.3−2326e	6.527	-0.251	50.20	W 28	snr	Disk	0.39
J1805.6−2136e	8.606	-0.211	160.43	W 30	snr	Disk	0.37
J1824.5−1350e	17.569	-0.452	266.09	HESS J1825−137	pwn	2D Gaussian	0.75
J1834.9−0848e	23.216	-0.373	67.30	W 41	spp	2D Gaussian	0.23
J1836.5−0655e	25.081	0.136	62.72	HESS J1837−069	pwn	Disk	0.33
J1840.9−0532e	26.796	-0.198	163.15	HESS J1841−055	pwn	Elliptical 2D Gaussian	0.62, 0.38, 39
J1923.2+1408e	49.112	-0.466	44.60	W 51C	snr	Elliptical Disk	0.38, 0.26, 90
J2021.0+4031e	78.241	2.197	115.97	Gamma Cygni	snr	Disk	0.63
J2028.6+4110e	79.601	1.396	28.09	Cygnus Cocoon	sfr	2D Gaussian	3.0

Note. — List of the 20 extended sources in the 2FHL that were previously detected as extended by the *Fermi*-LAT. All these sources are in 3FGL except W41, which is studied by Abramowski et al. (2015b). The Galactic coordinates l and b are given in degrees. The extension of the disk templates is given by the radius, the extension of the 2D Gaussian templates is given by the 1σ radius, and the elliptical templates are given by the semi-major axis, semi-minor axis, and position angle (East of North).

Table 7.2.   New 2FHL extended sources

2FHL Name	l [deg]	b [deg]	TS	TS_{ext}	TS_{2pts}	F_{50}	ΔF_{50}	Γ	$\Delta\Gamma$	Association	Class	Radius [deg]
J0431.2+5553e	150.384	5.216	87.9	83.4	26.2	11.70	2.11	1.66	0.20	G 150.3+4.5	snr	1.27
J1112.4−6059e	291.222	-0.388	80.9	68.3	22.5	12.80	2.36	2.15	0.28	PSR J1112−6103	pwn	0.53
J1355.2−6430e	309.730	-2.484	82.3	31.8	12.9	9.59	1.95	1.56	0.22	PSR J1357−6429	pwn	0.57
J1419.2−6048e	313.432	0.260	109.3	49.1	15.6	17.60	2.80	1.87	0.19	PSR J1420−6048	pwn	0.36
J1443.2−6221e	315.505	-2.239	75.6	29.9	19.2	7.23	1.70	2.07	0.30	SNR G315.4−2.3	snr	0.27

Note. — List of the 5 new extended sources in the 2FHL. All these sources are characterized by an uniform disk template whose radius is given in the last column.
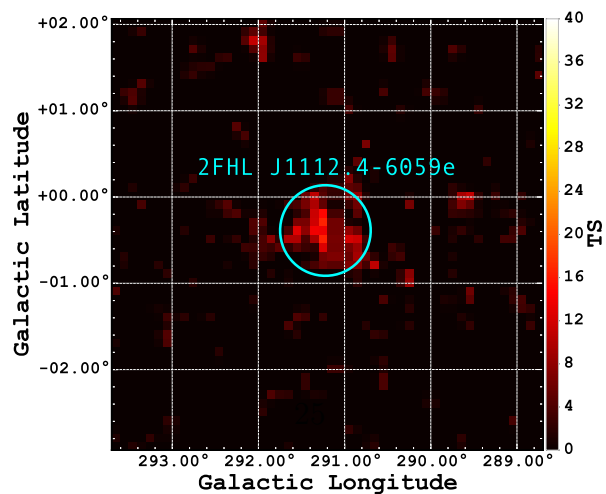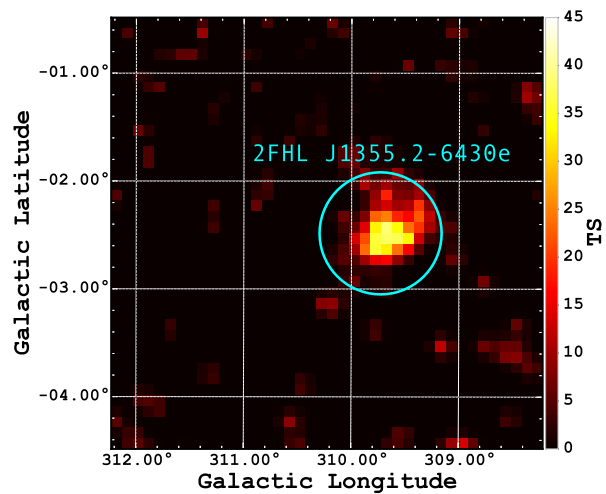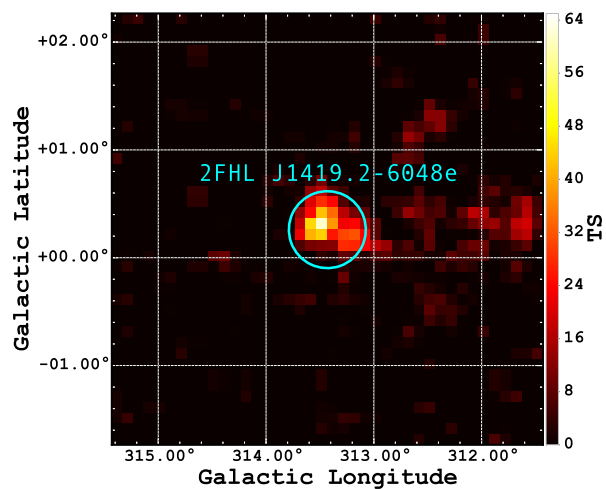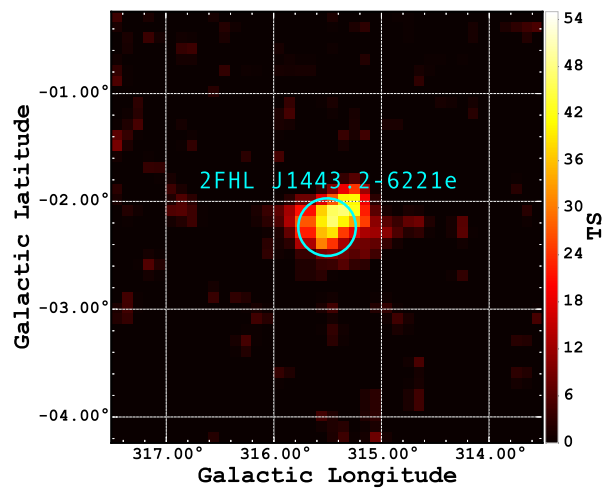
Chapter 8

SNR G150.3+4.5

Dedicated analysis of one interesting 2FHL result. First blindly detected extended γ-ray source. Large size + HI suggest it's near, hard spectrum looks like pwn, but size matches with radio SNR.

Take this all straight from the paper I write.

Chapter 9

SNR-MC, 10 GeV, and anything

else?

Not sure how this is going to factor in yet. SNR-MC should fit in somehow since a good deal of work was done? Less certain about 10gev.

Chapter 10

Conclusions

Finally!

List of Symbols and Acronyms

RoI region of interest.

SNR-MC supernova remant molecular system.

Bibliography

Abdo, A. A., Ackermann, M., Ajello, M., et al. 2009, Science, 325, 840

Abdo, A. A., Ajello, M., Allafort, A., et al. 2013, ApJS, 208, 17

Abramowski, A., Acero, F., Aharonian, F., et al. 2011, A&A, 533, A103

Abramowski, A., Aharonian, F., Ait Benkhali, F., et al. 2015a, A&A, 574, A27

—. 2015b, A&A, 574, A27

Acero, F., Ackermann, M., Ajello, M., et al. 2013, ApJ, 773, 77

—. 2015, ArXiv:1501.02003, arXiv:1501.02003:1501.02003

Aharonian, F., Akhperjanian, A. G., Bazer-Bachi, A. R., et al. 2006, A&A, 456, 245

Aharonian, F., Akhperjanian, A. G., de Almeida, U. B., et al. 2009, ApJ, 692, 1500

Gao, X. Y., & Han, J. L. 2014, A&A, 567, A59

Gotthelf, E. V., & Halpern, J. P. 2008, ApJ, 681, 515

Hewitt, J. W., Acero, F., Brandt, T. J., et al. 2013, ArXiv e-prints:1307.6570,
    arXiv:1307.6570

Hewitt, J. W., & Fermi-LAT Collaboration. 2015, in American Astronomical Society
    Meeting Abstracts, Vol. 225, American Astronomical Society Meeting Abstracts,
    140.31

Kerr, M. 2010, PhD thesis, University of Washington, arXiv:1101.6072

Lande, J., Ackermann, M., Allafort, A., et al. 2012, ApJ, 756, 5

Lemoine-Goumard, M., Renaud, M., Vink, J., et al. 2012, A&A, 545, A28

Lemoine-Goumard, M., Zavlin, V. E., Grondin, M.-H., et al. 2011, A&A, 533, A102

Roberts, M. S. E., Romani, R. W., Johnston, S., & Green, A. J. 1999, ApJ, 515, 712

Rosado, M., Ambrocio-Cruz, P., Le Coarer, E., & Marcelin, M. 1996, A&A, 315, 243

Sollerman, J., Ghavamian, P., Lundqvist, P., & Smith, R. C. 2003, A&A, 407, 249